Investigation on Deposit Formation during Low Load Operation of High Supercharged Diesel Engines

P.Eilts

Institut für Kolbenmaschinem
Universität Hannover
Welfengarten 1 A
D-3000 Hannover 1
F.R.Germany

ABSTRACT

Deposit formation during low load operation of high supercharged diesel engines can reduce reliability. Tests were run on a research engine to investigate the influence of constructive and operational parameters and to get information about the mechanisms causing deposit formation. In order to explain the tendencies measured a phenomenological model of the fuel jet was developed. It is possible to correlate the deposit masses measured with piston temperature and with the calculated fuel concentration on the jet centerline at the point of impact. Measures to reduce deposit formation are given.

INTRODUCTION

Deposit formation in the combustion chamber, charge air and exhaust system of high supercharged direct injection diesel engines during long low load operation can cause serious damages (1). It occurs especially with heavy fuel operation, but also with gas oil operation. An excessive amount of fuel on the combustion chamber walls is supposed to be the cause (1). The investigations described were made for clarification of the processes and for derivation of countermeasures.

EXPERIMENTAL INVESTIGATIONS

Test Procedure

Tests with a duration of 8h were run on an AVL engine (B = 0.12 m, s = 0.12 m). The engine had a low compression ratio (CR = 9.8) and was equipped with an external supercharger. It was operated on gas oil. In addition to the data necessary for supervision the piston temperature was measured. After the end of each run the engine was disassembled and the deposits were scraped off, weighed and analyzed chemically. A subdivision was made between piston bowl, squish area and top land. In the figures the respective area's percentage of the total mass is given. A list of all parameter constellations investigated is given in appendix A.

Experimental results

The deposit masses are well reproducible, with respect to the accuracy normally obtained in such investigations. The spread is indicated in the figures in case the same parameter constellation has been run several times. For the curves and percentages the average value was used. The mass-time-curve can approximately be descriped by a function of the type $m_{Dep} = k \cdot (1 - e^{-t/T})$. Time constants were in the range of 2 ... 20 h.

Further, the results of the parameter constellations investigated will be represented, in the order of the deposit reducing efficacy of the measures.

Deposit mass is reduced most by raising the compression ratio (Fig. 1).

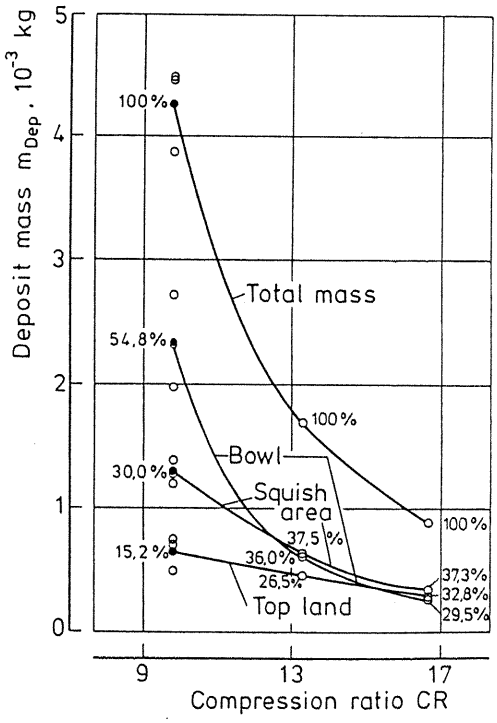

n = 1500 min^{-1} p_{me} = 0.185 MPa

Fig. 1 Variation of compression ratio

Very positive as well works an increase in charge air pressure, especially when the exhaust back pressure is increased at the same time (Fig. 2). This could be done by sequential supercharging.

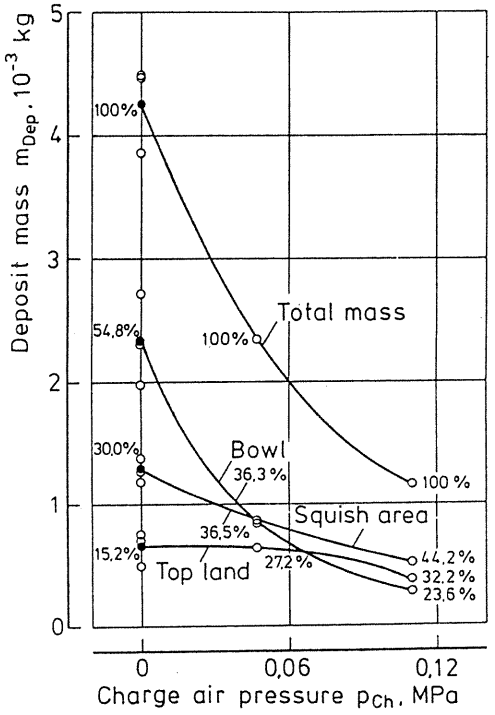

n = 1500 min^{-1} p_{me} = 0.185 MPa p_{Ex} = 0.9 p_{Ch}

Fig. 2 Variation of charge air pressure

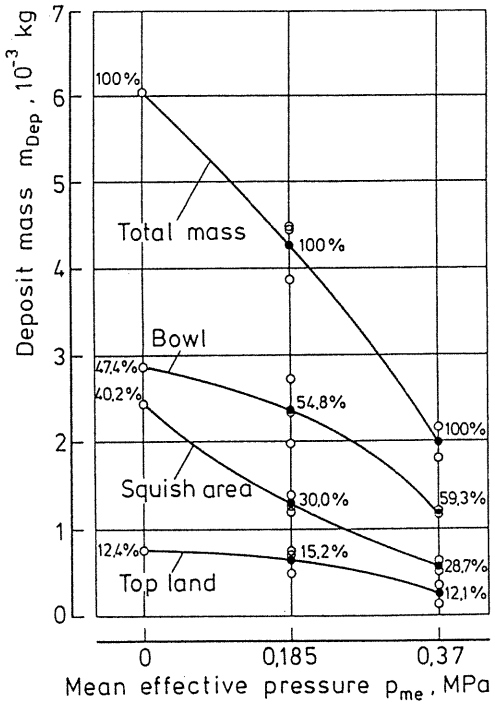

n = 1500 min^{-1}

Fig. 3 Variation of load

Higher load, e.g. by cylinder cutout, also significantly reduces deposit formation (Fig. 3). Higher speed works into the same direction, but less pronounced.

Raising the temperatures of oil and water only causes a small, positive trend. Higher charge air temperature works better, but only up to a certain value. After having attained that value, practically no further improvement is evident (Fig. 4).

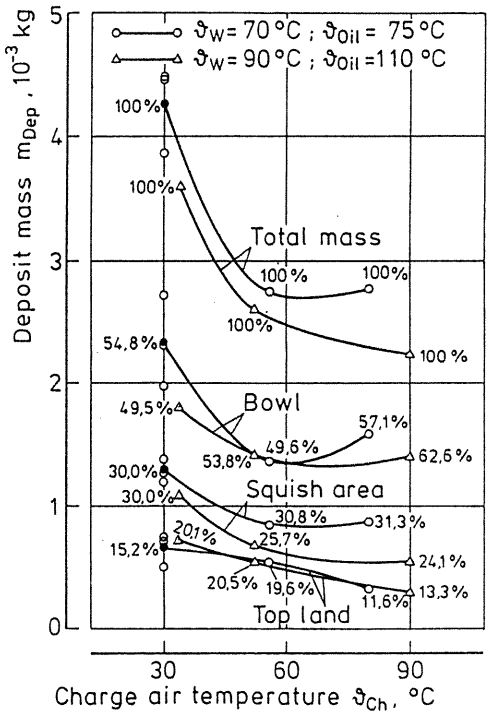

n = 1500 min^{-1} p_{me} = 0.185 MPa

Fig. 4 Variation of temperatures

Modifications of the injection system show minor improvements. Reducing the diameter of the nozzle holes does not bring the expected amelioration, at least not in the range investigated (50 ...150 % of the original cross section). Advancing fuel injection timing indicates a positive trend. Lower nozzle opening pressure causes a deterioration but higher opening pressure causes no improvement.

THEORETICAL WORK

Deposit masses were found to correlate well with Hydrocarbon emissions from the same engine (2), Fig. 5. As high HC-values had been shown to be caused by excessive wall wetting (2), it seemed probable that the same mechanism was the reason for deposit formation. This was confirmed by gas-chromatography, because high-boiling fractions of the fuel were found in the deposits.

First an attempt was made to correlate the measurements with the amount of non-evaporated fuel coming close to the wall. This aproach was not successfull, since in the short time it takes the jet to reach the wall only a small part of the

fuel evaporates, especially in the core of the jet, which mainly contributes to the wall film. So the explanation had to be looked for in the evaporation process on the wall.

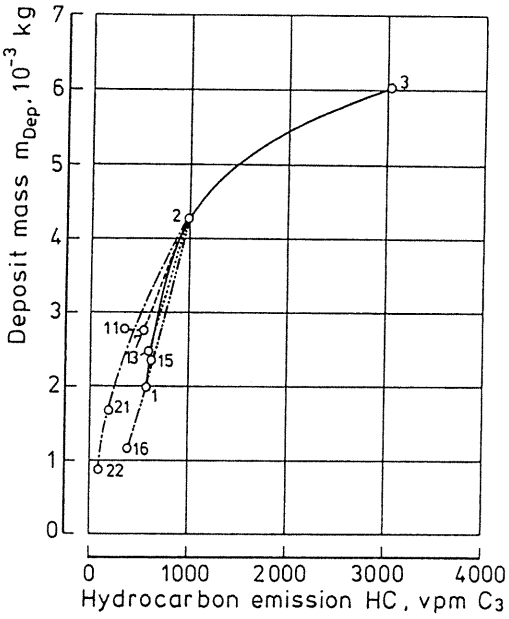

The figures indicate parameter constellations

Fig. 5 Correlation with HC-emission

In Fig. 6 measured deposit masses are plotted vs. piston temperature. For the points collected in the band a-a, a clear tendency showing lower deposit mass with rising piston temperature is evident. But there are some points falling out of this band. This only can be explained by differences in the formation of the fuel film and it's tendency to evaporate. A quantity describing this had to be found. For this purpose a phenomenological model of the fuel jet was developed. Like similar models of other authors (3) it is based on the theory of turbulent steady gas or liquid jets (4).

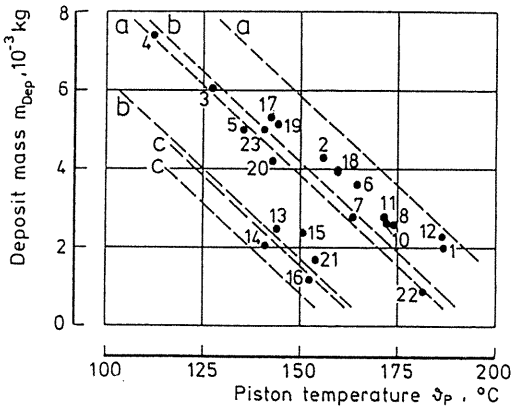

The figures indicate parameter constellations

Fig. 6 Correlation with piston temperature

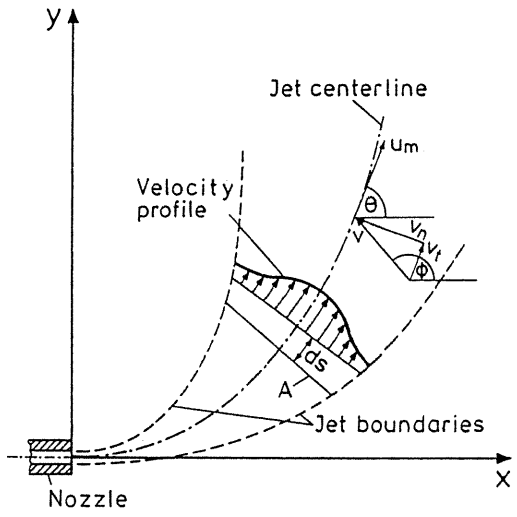

Fig. 7 Schematic of the jet model

Description Of The Model

The system considered is shown in Fig. 7. The following assumptions are made:

- The jet is slender, velocities are parallel to the centerline.
- Pressure is uniform over cross sections and depends on the external flow field according to Bernoulli's equation.
- The flow is incompressible.

The following equations can be written:

Conservation of fuel mass:

$$\dot{m}_f = \text{const.} \tag{1}$$

Conservation of momentum in x-direction:

$$\frac{d\dot{I}_x}{ds} = (v\cdot\cos\varphi\cdot\frac{d\dot{m}}{ds} - R\cdot c_d\cdot\varrho_a\cdot v_n\cdot|v_n|\cdot\sin\theta - A\cdot\frac{dp_{stx}}{ds})\cdot\sin\gamma \tag{2}$$

The equation in y-direction is written analogous. The terms on the right hand side represent momentum exchange by mass entrainment, the deviating force created by the external flow field and momentum transfer by change of the static pressure.

Change of jet radius or boundary layer thickness:

$$\frac{dR}{ds} = \frac{\alpha\cdot|u_m - v_t| + \lambda\cdot|v_n|}{\overline{u}},\quad \overline{u} = \frac{\varrho_m\cdot u_m + \varrho_a\cdot v_t}{\varrho_m + \varrho_a} \tag{3}$$

In the initial region the same expression is used for $d(R-R_c)/ds$.

Movement in x-direction:

$$\frac{dx}{ds} = \cos\theta \cdot \sin\gamma \qquad (4)$$

In y-direction a similar equation is valid.

These equations represent a system of ordinary differential equations, which must be solved numerically. The derivation of mass flux needed for the momentum equations is not available explicitly and has to be calculated numerically. This is done simultaneous with the integration using a simple difference quotient.

The profiles used are of the type $f=(1-\varepsilon^{1.5})^n$ (4). They are characterized by the parameter n or by the half-value thickness $\varepsilon_{1/2}$. In the initial region: $\varepsilon_{1/2u} = \varepsilon_{1/2c} = 0.559$. In the main region: $\varepsilon_{1/2u} = 0.441$ and $\varepsilon_{1/2c} = 0.630$ (4). In the transition region half-value thicknesses are interpolated linearly:

$$\varepsilon_{1/2} = (\varepsilon_{1/2M} - \varepsilon_{1/2I}) \cdot \eta \cdot s_{rel} + \varepsilon_{1/2I} \qquad (5)$$

$$s_{rel} = \frac{s - l_I}{d_n \cdot (\varrho_f/\varrho_a)^{1/2}} \qquad (6)$$

An unsteady (starting) jet consists of a steady jet with a head vortex or jet front (5). So the steady theory can be used if only a method is found which describes the behavior of the jet front. In the model used here a plain jet front is assumed. The jet front velocity is then obtained from a simple continuity consideration (3). The jet must grow as much as fuel is fed into it via the nozzle.

A mixture of liquid and vaporized fuel is assumed to emerge from the nozzle filling the whole cross sectional area (6). The velocity is set equal to the one achieved in the vena contracta (7).

Using this model a satisfactory agreement with measurements taken from the literature is obtained. More details are given in appendix B.

Correlation With Deposit Masses

The fuel concentration on the jet centerline at the point of impact C_{mimp} was found to be a quantity suitable to describe the formation of the wall film. In Fig. 8 the deposit masses are plotted vs. C_{mimp}. It can be seen that the points falling into band a-a in Fig. 6 have similar values of C_{mimp}. Furthermore the points falling out of band a-a can be collected in two more bands b-b and c-c by using Fig. 8. The tendency of a certain parameter constellation to form deposits can thus be predicted from the piston temperature and fuel concentration at the wall.

Using Figs. 6 and 8 the mechanism responsible for the observed tendency can be detected. In the following the parameter constellations are sorted with the varied parameter rising. Number 2 is the reference parameter constellation. Unfortunately piston temperatures are not available for all cases.

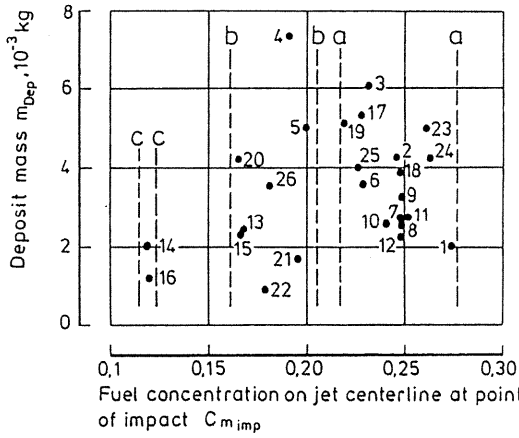

The figures indicate parameter constellations

Fig. 8 Correlation with fuel concentration

It can be seen that the improvements from rising load (parameter constellations 3-2-1) and temperatures (2-6-7-8-9-10-11-12) are due to a rise in piston temperature. With the advance of injection timing (17-2-18) temperature also plays the main role. On the contrary changes of charge air and exhaust gas pressure (2-13-15-14-16) mainly work via a reduction of C_{mimp}. A combined influence is found with the variation of speed (5-3-4), nozzle opening pressure (19-2-20), nozzle hole diameter (23-24-2-25-26) and compression ratio (2-21-22).

CONCLUSIONS

Measurements of deposit formation in a direct injection diesel engine during low load operation are presented. An effective reduction of deposit formation is possible by increasing the compression ratio, the charge air and exhaust gas pressure (e.g. by sequential supercharging) and the load (e.g. by cylinder cutout). Higher temperatures also are advantageous, depending on the starting level. The deposits in the tests described in this work were probably formed mainly from fuel that had been deposited on the wall in the liquid state and evaporated incompletely. The deposit mass can be correlated with piston temperature and the fuel concentration on the jet centerline at the point of impact.

NOMENCLATURE

A	jet cross sectional area, m^2
B	cylinder bore, m
bod	begin of delivery, °CA
C	fuel concentration
c_d	drag coefficient
CR	compression ratio
d_n	nozzle hole diameter, m
f	value of distribution profile
HC	hydrocarbon emission, vpm C_3
$\dot{I}$	momentum flux, N
k	constant, kg
l_I	length of initial region, m
l_n	nozzle hole length, m
n	parameter in distribution profile
n	engine speed, min^{-1}
m	mass, kg
$\dot{m}$	mass flux, kg/s

p_{ch} charge air pressure, MPa
p_{Ex} exhaust gas pressure, MPa
p_{me} mean effective pressure, MPa
p_o nozzle opening pressure, MPa
p_{st} static pressure, Pa
R jet radius, m
R_c radius of potential core, m
s jet path, m
s piston stroke, m
s_{rel} dimensionless jet path in transition region
t time, h
T time constant, h
u velocity in the jet, m/s
v velocity of the external flow field, m/s
x x-coordinate, m
y y-coordinate, m
α empirical parameter
γ angle between centerline and z-axis, rad
ε dimensionsless thickness/radius
$\varepsilon_{1/2}$ half-value thickness/radius
η empirical parameter
ϑ_{ch} charge air temperature, °C
ϑ_{oil} oil inlet temperature, °C
ϑ_W cooling water inlet temperature, °C
ϑ_P piston temperature, °C
θ angle betwenn centerline and x-axis, rad
λ empirical parameter
ϱ density, kg/m³
ϕ angle between v-vector and x-axis, rad

Subscripts

a of air
C for concentration
Dep of deposit
f of fuel
I in initial region
imp at point of impact
m maximum, on jet centerline
M in main region
n normal to jet centerline
t tangential to jet centerline
u for velocity
x in x-direction
y in y-direction

ACKNOWLEDGEMENT

The author wishes to thank Prof. Dr.-Ing. K. Groth, Director of the Institute for Reciprocating Machines, University of Hannover, for the support of the work described in this paper.

REFERENCES

1. Borchsenius, H. J. and Zapf, H., "Viertakt-M.A.N.-B&W-Motoren im Teillastbetrieb," HANSA, 121. Jahrgang, Nr. 10, 1984.
2. Sprogis, W.A., Der Einfluß des Verdichtungsverhältnisses auf die Gesamtkohlenwasserstoff-Emission eines direkteinspritzenden Dieselmotors, Dissertation, Universität Hannover, 1983.
3. Meguerdichian, M. and Watson, N., "Prediction of Mixture Formation and Heat Release in Diesel Engines," SAE-Paper 780225, 1978.
4. Abramovich, G. N., The Theory of Turbulent Jets, MIT-Press, Cambridge, 1963.
5. Bracco, F. V., "Modeling of Engine Sprays," SAE-Paper 850394, 1985.
6. Schmitt, T., Untersuchungen zur stationären und instationären Strömung durch Drosselquerschnitte in Kraftstoffeinspritzsystemen von Dieselmotoren, Dissertation, Technische Hochschule München, 1966.
7. Schaffitz, W. and Bauer, W., "Rechenmodell Strahlausbreitung," Forschungsberichte Verbrennungskraftmaschinen, Heft 367, Forschungsvereinigung Verbrennungskraftmaschinen, Frankfurt a. M., 1985.
8. de Neef, A. T. , Untersuchung der Voreinspritzung am schnellaufenden, direkteinspritzenden Dieselmotor, Dissertation, ETH Zürich, 1987.

APPENDIX A
LIST OF PARAMETER CONSTELLATIONS

The reference parameter constellation is characterized by the following data:

Compression ratio	CR	= 9.8
Speed	n	= 1500 min^{-1}
Mean effective pressure	p_{me}	= 0.185 MPa
Naturally aspirated		
Charge air temperature	ϑ_{ch}	= 30 °C
Oil inlet temperature	ϑ_{oil}	= 75 °C
Cooling water inlet temperature	ϑ_W	= 70 °C
nozzle hole diameter	d_n	= 0.33 mm
begin of delivery	bod	= 33 °CA
nozzle opening pressure	p_o	= 24 MPa

In the following all parameter constellations are listed. Only the data changed with respect to the reference parameter constellation are given.

parameter constellation	data
1	p_{me} = 0.37 MPa
2	reference parameter constellation
3	p_{me} = 0 MPa
4	p_{me} = 0 MPa, n = 1000 min^{-1}
5	p_{me} = 0 MPa, n = 2000 min^{-1}
6	ϑ_W = 90 °C, ϑ_{oil} = 110 °C
7	ϑ_{ch} = 55 °C
8	ϑ_{ch} = 55 °C, ϑ_W = 90 °C
9	ϑ_{ch} = 55 °C, ϑ_{oil} = 110 °C
10	ϑ_{ch} = 55 °C, ϑ_W = 90 °C, ϑ_{oil} = 110 °C
11	ϑ_{ch} = 80 °C
12	ϑ_{ch} = 90 °C, ϑ_W = 90 °C, ϑ_{oil} = 110 °C
13	p_{CH} = 0.05 MPa, p_{Ex} = 0.0 MPa (superpressure)
14	p_{CH} = 0.11 MPa, p_{Ex} = 0.0 MPa (superpressure)
15	p_{CH} = 0.05 MPa, p_{Ex} = 0.045 MPa (superpressure)
16	p_{CH} = 0.11 MPa, p_{Ex} = 0.1 MPa (superpressure)
17	bod = 28 °CA
18	bod = 37 °CA
19	p_o = 12 MPa
20	p_o = 36 MPa
21	CR = 13.3, bod = 28 °CA
22	CR = 16.7, bod = 25 °CA
23	d_n = 0.4 mm
24	d_n = 0.37 mm
25	d_n = 0.29 mm
26	d_n = 0.23 mm

APPENDIX B
DETAILS OF THE JET MODEL

Solution Of The Equations

In the following the procedure used for solution of the differential equations given above is described.

Fuel mass flux, total mass flux and momentum flux are given in an integral form:

Fuel mass flux:

$$\dot{m}_f = \int_A C \cdot \varrho \cdot u \cdot dA \tag{7}$$

Total mass flux:

$$\dot{m} = \int_A \varrho \cdot u \cdot dA \tag{8}$$

Momentum flux:

$$\dot{I} = \int_A \varrho \cdot u^2 \cdot dA \tag{9}$$

Additional equations are:

Momentum flux in x- and y-direction:

$$\dot{I}_x = \dot{I} \cdot \cos\theta \cdot \sin\gamma \tag{10}$$

$$\dot{I}_y = \dot{I} \cdot \sin\theta \cdot \sin\gamma \tag{11}$$

Velocity in the jet:

$$u = v_t + (u_m - v_t) \cdot f_u(\varepsilon) \tag{12}$$

Concentration in the jet:

$$C = C_m \cdot f_c(\varepsilon) \tag{13}$$

Here $f_u(\varepsilon)$ and $f_c(\varepsilon)$ are the values of the dimensionless distribution profiles given above.

Density in the jet:

$$\varrho = \frac{\varrho_a}{1 - C \cdot (1 - \varrho_a/\varrho_f)} = \frac{\varrho_a}{1 - C_m \cdot f_c \cdot \beta} \tag{14}$$

The further prodecure will be indicated for the transition and main region. Using the dimensionless radius ε we get:

$$dA = 2 \cdot \pi \cdot R^2 \cdot \varepsilon \cdot d\varepsilon \tag{15}$$

With equations 12 to 15 equation 7 for the fuel mass flux becomes:

$$\dot{m}_f = \varrho_a \cdot 2 \cdot \pi \cdot R^2 \cdot \left(v_t \cdot \int_0^1 \frac{f_c \varepsilon d\varepsilon}{1 - C_m \beta f_c} + (u_m - v_t) \cdot \int_0^1 \frac{f_c f_u \varepsilon d\varepsilon}{1 - C_m \beta f_c} \right) \tag{16}$$

Equation 9 for the momentum flux is manipulated in the same way. Now u_m and C_m can be calculated from $\dot{I}$ and $\dot{m}_f$. These two equations have to be solved simultaneously in an iterative procedure, since C_m appears in the integrals. The angle θ is calculated from equations 10 and 11.

In the initial region R_c is calculated from $\dot{m}_f$. The conservation-equation of momentum is not needed explicitly here. To satisfy it, the profiles for velocity and concentration have to be adapted adequately. This is done simplest, if they are chosen to be identical. The resulting profiles are given above. They fit experimental data from gas jets given by Abramovich (4) quite well.

It was said above that the derivation of mass flux needed for the momentum equations is obtained numerically. This method is quite unusual. The normal way would have been to differentiate the equations and solve the resulting system for the derivations of u_m, C_m and θ instead of $\dot{I}_x$ and $\dot{I}_y$ (in the transition and main region). This method is suggested in the literature. It's first disadvantage is the relative complicatedness of the program. The second and more important is the resulting of a stiff system, because u_m and C_m change much faster than the other variables integrated. So this path was left after initial trials because of numerical difficulties. The accuracy of the method proposed is sufficient to keep numerical losses of excess momentum of a jet in a coflowing stream less than 1% after 500 nozzle diameters.

Experimental constants

The constant α is dependent of the ratio l_n/d_n, as jet angle is. For a nozzle with l_n/d_n = 3.2, α = 0.1 was found. The formula for the dependence of jet angle given by de Neef (8) is used to calculate the dependence of α on l_n/d_n. The other parameters are: λ = 0.19, c_d = 1.6 and η = 0.15.

Comparison with measurements

As an example for the accuracy obtained fuel distributions measured by (7) are compared with a calculated curve in Fig. 9. The good agreement which is obtained also at different back pressures and distances from the nozzle indicates that gas jet profiles are applicable even to non-evaporating fuel sprays.

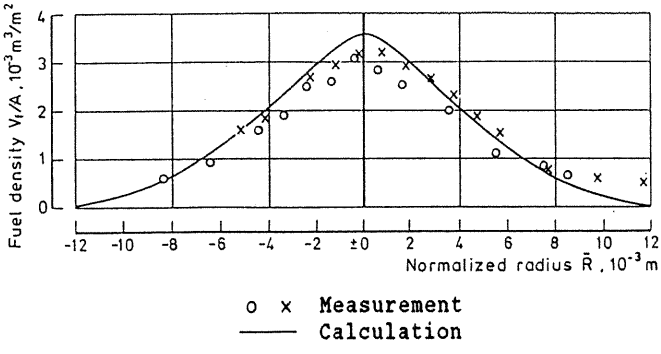

Fig. 9 Comparison of measurement and calculation